

Large-scale particle trapping by acoustic vortices with a continuously variable topological charge

Haofei Zhuang(庄昊霏), Qingyuan Zhang(张清源), Gehao Hu(胡格昊), Qingdong Wang(王青东), and Libin Du(杜立彬)

Citation: Chin. Phys. B, 2024, 33 (**7**): 074302. DOI: 10.1088/1674-1056/ad5aef
Journal homepage: http://cpb.iphy.ac.cn; http://iopscience.iop.org/cpb

What follows is a list of articles you may be interested in

Helical particle manipulation based on power-exponent-phase acoustic vortices generated by a sector transducer array

Qingdong Wang(王青东), Yantao Hu(胡彦涛), Shengli Wang(王胜利), and Hongyu Li(李洪宇)
Chin. Phys. B, 2023, 32 (**6**): 064304. DOI: 10.1088/1674-1056/acc800

Controlling acoustic orbital angular momentum with artificial structures: From physics to application

Wei Wang(王未), Jingjing Liu(刘京京), Bin Liang (梁彬), and Jianchun Cheng(程建春)
Chin. Phys. B, 2022, 31 (**9**): 094302. DOI: 10.1088/1674-1056/ac7868

Measuring orbital angular momentum of acoustic vortices based on Fraunhofer's diffraction

Chao-Fan Gong(龚超凡), Jing-Jing Li(李晶晶), Kai Guo(郭凯), Hong-Ping Zhou(周红平)†, and Zhong-Yi Guo(郭忠义)‡
Chin. Phys. B, 2020, 29 (**10**): 104301. DOI: 10.1088/1674-1056/ab9c11

Random phase screen influence of the inhomogeneous tissue layer on the generation of acoustic vortices

Zhiyao Ma(马致遥), Jun Ma(马骏), Dong Zhang(章东), Juan Tu(屠娟)
Chin. Phys. B, 2018, 27 (**3**): 034301. DOI: 10.1088/1674-1056/27/3/034301

Multiple off-axis acoustic vortices generated by dual coaxial vortex beams

Wen Li(李雯), Si-Jie Dai(戴思捷), Qing-Yu Ma(马青玉), Ge-Pu Guo(郭各朴), He-Ping Ding(丁鹤平)
Chin. Phys. B, 2018, 27 (**2**): 024301. DOI: 10.1088/1674-1056/27/2/024301

Large-scale particle trapping by acoustic vortices with a continuously variable topological charge

Haofei Zhuang(庄昊霏)[3], Qingyuan Zhang(张清源)[2], Gehao Hu(胡格昊)[3], Qingdong Wang(王青东)[1,†], and Libin Du(杜立彬)[1]

[1] *College of Ocean Science and Engineering, Shandong University of Science and Technology, Qingdao* 266590, *China*
[2] *Department of Radiology, the Affiliated Hospital of Qingdao University, Qingdao* 266000, *China*
[3] *College of Electronic and Information Engineering, Shandong University of Science and Technology, Qingdao* 266590, *China*

(Received 29 April 2024; revised manuscript received 14 June 2024; accepted manuscript online 24 June 2024)

Strengthened directivity with higher-order side lobes can be generated by the transducer with a larger radius at a higher frequency. The multi-annular pressure distributions are displayed in the cross-section of the acoustic vortices (AVs) which are formed by side lobes. In the near field, particles can be trapped in the valley region between the two annuli of the pressure peak, and cannot be moved to the vortex center. In this paper, a trapping method based on a sector transducer array is proposed, which is characterized by the continuously variable topological charge (CVTC). This acoustic field can not only enlarge the range of particle trapping but also improve the aggregation degree of the trapped particles. In the experiments, polyethylene particles with a diameter of 0.2 mm are trapped into the multi-annular valleys by the AV with a fixed topological charge. Nevertheless, by applying the CVTC, particles outside the radius of the AV can cross the pressure peak successfully and move to the vortex center. Theoretical studies are also verified by the experimental particles trapping using the AV with the continuous variation of three topological charges, and suggest the potential application of large-scale particle trapping in biomedical engineering.

Keywords: acoustic vortices, sector transducer array, trapping particle, continuously variable topological charge

PACS: 43.72.+q, 43.38.Hz **DOI:** 10.1088/1674-1056/ad5aef

1. Introduction

Objects of different shapes and materials in the liquid[1] and in the air[2–4] can be manipulated by the acoustic wave. The objects such as high-density materials,[5] high temperature liquid[6] and live small animals[7] can be controlled by the acoustic field generated by the standing wave.[3,8] However, another acoustic field has attracted more and more attention from researchers, which is characterized by a screw phase dislocation around its propagation axis[9] and a null pressure magnitude at the field center.[10,11] They are acoustic vortices (AVs)[12,13] that can be used to rotate and gather small objects. The spiral phase singularity of the acoustic wave propagation was reported for the first time by J. Nye and M. Berry.[12] The orbital angular momentum carried by the AV was transferred to matters in the free sound field[14,15] in theoretical derivations[16,17] and experimental measurements.[18] Many investigations showed that the objects in the sound field are moved and rotated by the action of acoustic radiation force and torque.[19–22]

All these intriguing properties of AVs have spurred many efforts to investigate them to obtain advanced applications of AVs. The theory of acoustical radiation of phase-coded point source was proposed by Yang and Ma to generate controllable AV.[23] It was also proved that more circular pressure distributions[24] of AVs with higher peak pressure and lower pressure fluctuation could be generated by more sources, and improved linearity[25] of circular phase distributions could be produced by more sources at lower frequencies with a smaller vortex radius. The AVs with different topological charges were presented,[26,27] and with an increase in topological charges, the radius of AVs increased. Acoustic vortices using sparse directional planar piston sources were proposed with explicit formulae,[28] but the side-AV was produced by the side lobes at a relatively lower pressure. In order to increase the side lobes pressure, a sector transducer array was employed for generating AVs.[29,30] In addition, focused AVs were generated by phased array systems[31] or focused transducer[18] to obtain much higher pressure. The AVs mentioned above were generated by the elements of the transducer array excited by phase or amplitude-modulated signals. Furthermore, some specific structures were designed to produce customized AVs;[32–34] e.g., a periodically structured stiff plate[35] and a structured brass plate[36] with Archimedean spiral grating. However, once the structures are set, the topological charges of the AVs cannot be adjusted easily by simple post-processing. No matter which method is used to generate the AV, the pressure on the cross-section of the vortex will form the annular distributions.

An important application of AV is to manipulate objects. A vortex field was generated and manipulated by a 16-element

[†]Corresponding author. E-mail: wangqingdong@sdust.edu.cn

© 2024 Chinese Physical Society and IOP Publishing Ltd

ultrasound array which formed a circular chamber. It was reported by C. R. P. Courtney *et al.* in 2013.[37] In order to improve the dexterity, the way of increasing the number of elements was introduced by them in 2014. The acoustic tweezers consist of a circular 64-element ultrasonic array operating at 2.35 MHz which generates ultrasonic pressure fields in a millimeter-scale fluid-filled chamber.[38] Reducing the order of the Bessel function reduces the radius of the first peak and the size of the central trap, and particles can be progressively forced to the vortex center, so the radius of the largest trapping range is the distance from the first pressure peak to the vortex center. Based on the theory of Gor'kov potential, particles in AVs were demonstrated to move from high-pressure regions to low-pressure regions in a rotating mode.[3] Therefore, the particles located outside of the high-pressure rings cannot be trapped to the vortex center.

Coincidentally, multi-size particles were controlled by AVs in a chamber that consisted of 64 individually addressable piezoelectric sources arranged around a ring.[14] The fractional-order acoustic vortices generated by this ultrasound array were used to manipulate two single 90-μm diameter polystyrene microparticles in non-axisymmetric acoustic fields, in which the topological charge was fractional.[39] Axial radiation forces in the axial direction were offset by the interface of the chamber, the particles were trapped in a horizontal plane. The ultrasonic manipulation of particles and cells along a microfluidic channel was demonstrated by a 1-D piezoelectric array and a planar multilayer resonator structure.[40] The trapping of elastic particles by the high gradient force of a single acoustical beam has been demonstrated by Diego Baresch *et al.*[41] in three dimensions, regarding the particle size, beads up to a third of the wavelength in diameter were successively trapped, but larger ones were predicted to be expelled. The incident energy was distributed on a bigger surface ring and explained the lower gain factors with increasing topological charge.[42] So in order to improve the efficiency of trapping particles, the topological charge of the AV was set to $l = 8$, when the radius of the particle was equal to the wavelength.

In previous studies, the mechanisms underlying the generation of AVs were investigated based on multiple models with invariable topological charges. Meanwhile, the AVs offered a fixed-radius valley near the paraxial, which could be considered as the optimal potential well. However, for particles dispersed in a large region, such valley at the vortex center is too small to achieve large-region trapping particles. Despite that the large-scale potential wells of expanded AVs with reduced peak pressures were also demonstrated for a higher topological charge,[30] the particles outside the first pressure peak were still driven to move outward. Especially in the near field, although the acoustic potential and gradient force are higher, the multi-annulus peak pressure distributions formed by the AV with invariable topological charge will hinder the particles to move toward the vortex center. Therefore, in order to expand the trapping range, it is necessary to make the particles avoid the pressure peaks.

A new method for manipulating objects using AVs is presented in this paper. The acoustic vortices with continuously variable topological charges (CVTC) move particles to the vortex center and rotate them around the axis of AVs in large regions. Based on the acoustic radiation of point sources, the physical mechanism of AVs generated by sector transducers is investigated with formulae derivations of acoustic pressure. The numerical simulations of the acoustic fields with different topological charges are presented. The results show that with the increase of the topological charge, the first peaks of pressure and gradient force decrease accordingly with an enlarged radius of AV (or potential well), demonstrating a gradually dispersed main-lobe AV, and the multi-annular peak pressure formed by the side lobes hinders the movement of particles in the near field. In order to avoid the pressure peaks, the acoustic field with CVTC is introduced for the particles trapping in the larger region. In the new field, the particles can be moved from a longer radial distance to the vortex center. It is also an effective way to improve the aggregation degree of the trapped particles.

2. Principle and method

In the source plane, N sector planar piston sources with the radius $a = 40$ mm are distributed uniformly to form a complete circle, as shown in Fig. 1(a). The photo of the fabricated sector transducer array is displayed in Fig. 1(b), and the N sector elements are integrated into a steel structure. The spatial angle of each sector source is $\Delta\varphi = 2\pi/N$, and the color bar represents the initial phase of the vibration sources. The sector source is considered to be the accumulation of multiple point sources for the convenience of calculation. To generate the AV beam, the phase difference between the adjacent elements is set to $2\pi l/N$ to produce a total phase shift of $2\pi l$ for all sector transducers, where the integer l is topological charge or the order of the helicoidal beam and encodes the angular rotation rate of the wavefront.[14] Then the radiation acoustic pressure at the observation position excited by the sector transducer array can be calculated as

$$p(r_{\mathrm{o}}, \varphi_{\mathrm{o}}, z_{\mathrm{o}}) = \sum_{n=1}^{N} \frac{\mathrm{j}k\rho_{\mathrm{o}}c_{\mathrm{o}}}{2\pi} A_0 \int_0^a \int_{\varphi_n}^{\varphi_n+\Delta\varphi} \frac{\exp \mathrm{j}[(\omega t - kR_n - \phi_n)]}{R_n} r\,\mathrm{d}r\,\mathrm{d}\varphi, \tag{1}$$

where A_0 is the amplitude of vibration velocity and ω is the angular frequency, $\phi_n = 2\pi(n-1)/N$ is the initial phase of the nth vibration source. ρ_{o} and c_{o} are

the density and the acoustic speed of the medium, $k = \omega/c_o$ is the wave number of the acoustic wave. $R_n = \sqrt{[r_o\cos\varphi_o - r\cos\varphi]^2 + [r_o\sin\varphi_o - r\sin\varphi]^2 + z_o^2}$ is the transmission distance from the point $(r,\varphi,0)$ in the nth sector plane to viewing point (r_o,φ_o,z_o) and $t_n = R_n/c_o$ is the corresponding transmission time.

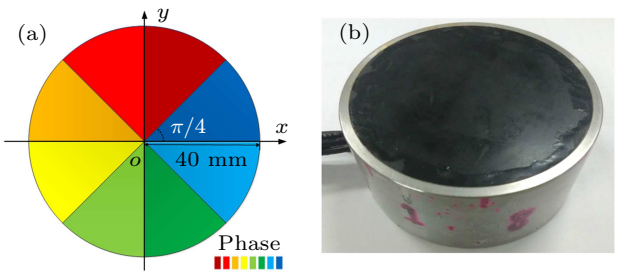


Fig. 1. (a) Sketch map of the 8-element sector transducer array with radius $a = 40$ mm. (b) Photo of the fabricated sector transducer array. Color bar represents the initial phase of the vibration sources.

Due to the acoustic pressure gradient of AVs, the particles are drafted by the gradient radiation force[43]

$$F = -\nabla U = -\pi a_p^3\left[\frac{(c_p^2\rho_p - c_o^2\rho_o)\nabla|p|^2}{3c_p^2\rho_p\rho_o c_o^2} - \frac{2(\rho_p-\rho_o)\rho_o\nabla|v_\perp|^2}{2(2\rho_p+\rho_o)}\right], \tag{2}$$

which is often employed to explain the movement of small objects in acoustic fields, where U is the Gor'kov potential, the subscripts 'o' and 'p' represent the medium and particle, respectively. The transverse particle velocity $v_\perp$ can be calculated by $\left(\hat{r}\frac{\partial p}{\partial r} + \hat{\varphi}\frac{1}{r}\frac{\partial p}{\partial \varphi}\right)/(\mathrm{j}\omega\rho)$.[15] Enhanced efficiency of trapping particles can be realized by the higher acoustic gradient force (AGF), and enlarged trapping region can be realized by the AV with strengthened CVTC in the near field. Throughout the paper, the MATLAB software is used for the numerical simulations.

3. Numerical studies

The directivity envelope of the transducer depends on the size and working frequency of the transducer,[44] and with increases in the size and frequency, the directivity becomes stronger. In this study, a sector transducer array with strong directivity is used to generate and control the acoustic field with higher side lobe pressure. In the near field, multiple annular AVs are formed by multi-order side lobes instead of the main lobe.[30] Based on the phase-coded approach, the mechanisms underlying the generation of lager region trapping particles of AVs using an 8-element sector transducer are proposed with explicit formulae. The pressure and AGF distributions of AVs with topological charges of 1, 2 and 3 are conducted. The drive signal of each element is the sinusoidal wave with a frequency of 500 kHz and an amplitude of 10 V, acoustic velocity c_o and density of water are set to be 1500 m/s and 1000 kg/m^3.

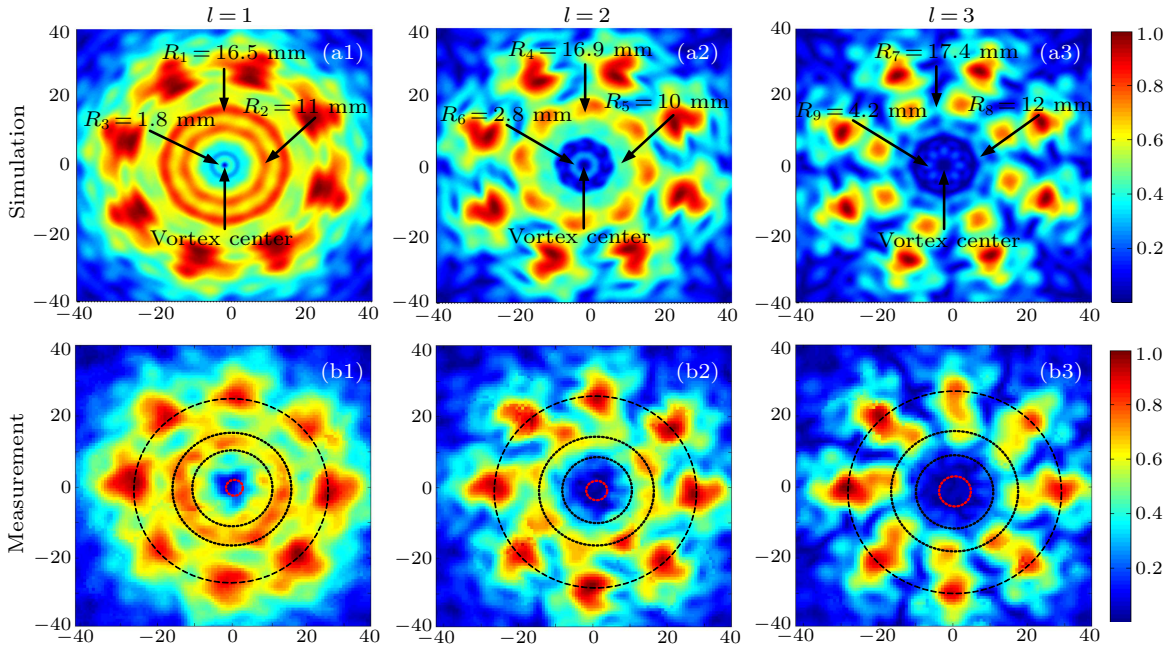


Fig. 2. (a1)–(a3) Numerical and (b1)–(b3) experimental transverse distributions of normalized pressure at $z = 65$ mm for AVs with $l = 1$, 2 and 3, respectively.

The 2D cross-sectional distributions of pressure generated by the sector transducer array are shown in Figs. 2(a1), 2(a2) and 2(a3) at the axial distance $z = 65$ mm. The radius of AV is defined as the distance from the vortex center to the peak pressure of AVs. As shown in Fig. 2(a), topological charge $l = 1$, with the increase of the radial radius, the normalized acoustic pressure increases accordingly from 0 to 0.5 at the radius of about $R_3 = 1.8$ mm. When the ra-

dial distance increases from $R_3 = 1.8$ mm to $R_2 = 11$ mm, the normalized acoustic pressure decreases to 0.31 and then increases to around 0.89. The particles in the region between $R_3 = 1.8$ mm and $R_2 = 11$ mm will be bound by the two annular peaks, and can not continue to move toward the vortex center. Furthermore, the particles are also trapped in the valley region between $R_2 = 11$ mm and $R_1 = 16.5$ mm. Likewise, this phenomenon will also occur in the AVs of topological charges $l = 2$ (Fig. 2(a2)) and 3 (Fig. 2(a3)), such as the valley regions between $R_6 = 2.8$ mm and $R_5 = 10$ mm and between $R_9 = 4.2$ and $R_8 = 12$ mm. The radius of the innermost layer vortex with the topological charge of 3 is 2.33 times (R_9/R_3) of the topological charge of 1. Therefore, the AVs with a high topological charge can be used to expand the region of the trapping particle. In contrast, AVs with a low topological charge are used to improve the aggregation degree of the trapped particles. The distance between the vortex center and the first pressure peak (the innermost layer AVs) increases with the increase of the topological charge, however, the pressure of the first peak will decrease, which will be presented in the next part.

The 2D distributions of experimental pressure are shown in Figs. 2(b1), 2(b2) and 2(b3), these data are collected by the hydrophone. When the topological charge is 1, three annular peak pressures are observed apparently at the radial radii of about 1.8 mm, 11 mm and 16.5 mm, and the pressure in the vortex center is almost zero. Due to the smaller area of the potential well at the vortex center, the precise trapping of objects can be realized. When the topological charge $l = 2$, irregular annular pressures at the radii of 2.8 mm, 10 mm and 16.9 mm formed by the side lobes are exhibited in the diagram of Fig. 2(b2), the area of the potential well in the paraxial region is larger than that in Fig. 2(b1). For $l = 3$, three circles of peak pressure at the radii of 4.2 mm, 12 mm and 17.4 mm are clearly displayed in Fig. 2(b3) with an obvious pressure null at the origin, the region of particles trapping is the largest. The side lobe AV at the radius of 17.4 mm splits and connects with the main lobe AV. Experimental results have a good agreement with the numerical results.

The acoustic field generated by the sector transducer array, with appropriate drive signals, is periodically changed the CVTC. The topological charge changes from $l = 3$ to 2 and then to 1, as a cycle. The particles in this acoustic field can be trapped into the vortex center with numerous cycles uninterruptedly. Two progressive characteristics of these AVs are the larger range of trapping particles and the stronger ability to cluster particles. The one-dimensional distributions of radial pressure for the three topological charges are shown in Fig. 3(a) at $z = 65$ mm. Due to the multi-order side lobes of the sector transducers, obvious fluctuations of acoustic pressure are clearly displayed in the near field, so particles are easily hindered in the valley between two peaks.

At a moment, assuming some particles are driven and confined in the valley (the radial distance $r_2 = 4.8$ mm, normalized pressure is 0.103) between $R_5 = 10$ mm and $R_6 = 2.8$ mm, as shown in Fig. 3(a), where the topological charge $l = 2$. At the next moment, the topological charge of the acoustic field is set as $l = 1$, and those particles (at $r = 4.8$ mm) are acted by high acoustic pressure (relative to the pressure at $r_1 = 3.4$ mm) at this time, so that the particles can continue to move to the next valley which is between $R_3 = 1.8$ mm and $R_2 = 11$ mm ($r_1 = 3.4$ mm, normalized pressure is 0.31). In order to move particles toward the vortex center, the topological charge is changed to 3 in the next moment. As well, once again the particles (at $r = 3.4$ mm) are driven by high acoustic pressure (relative to the pressure in the vortex center) in the field with $l = 3$. Due to the AVs with periodic CVTC, the particle with a larger radial distance can be moved to the vortex center, when the radius of the innermost layer AV is larger compared to the particle size.

The description of particle movements is presented in Table 1 in different time periods of the CVTC field. The distances between the start and end points from the vortex center (VC) are shown in millimeters. In the column of motion direction, the arrow-pointing-left symbol represents that the particles migrate in the direction of the vortex center, and the particles at rest are indicated by a '×' symbol in the radial direction.

Table 1. The displacement of particles.

Time	l	Start point	End point	Start pressure	End pressure	Motion direction
$0 \to t_1$	2	4.8 (r_2)	4.8 (r_2)	0.103	0.103	×
$t_1 \to t_2$	1	4.8	3.4 (r_1)	0.43	0.31	←
$t_2 \to t_3$	3	3.4	0 (VC)	0.3	0	←
$t_3 \to t_4$	2	0 (VC)	0 (VC)	0	0	×

With the increase of the topological charge, the first peak of radial pressure decreases accordingly with an enlarged radius. The radii of the innermost layer AVs are 1.8 mm, 2.8 mm and 4.2 mm, for the AVs with invariable topological charge, this is also the maximum radius of the trapping range corresponding to the topological charges of 1, 2 and 3, respectively. Nevertheless, it is inspiring that the maximum trapping radius of AVs with CVTC can be expanded to 17.4 mm at $z = 65$ mm.

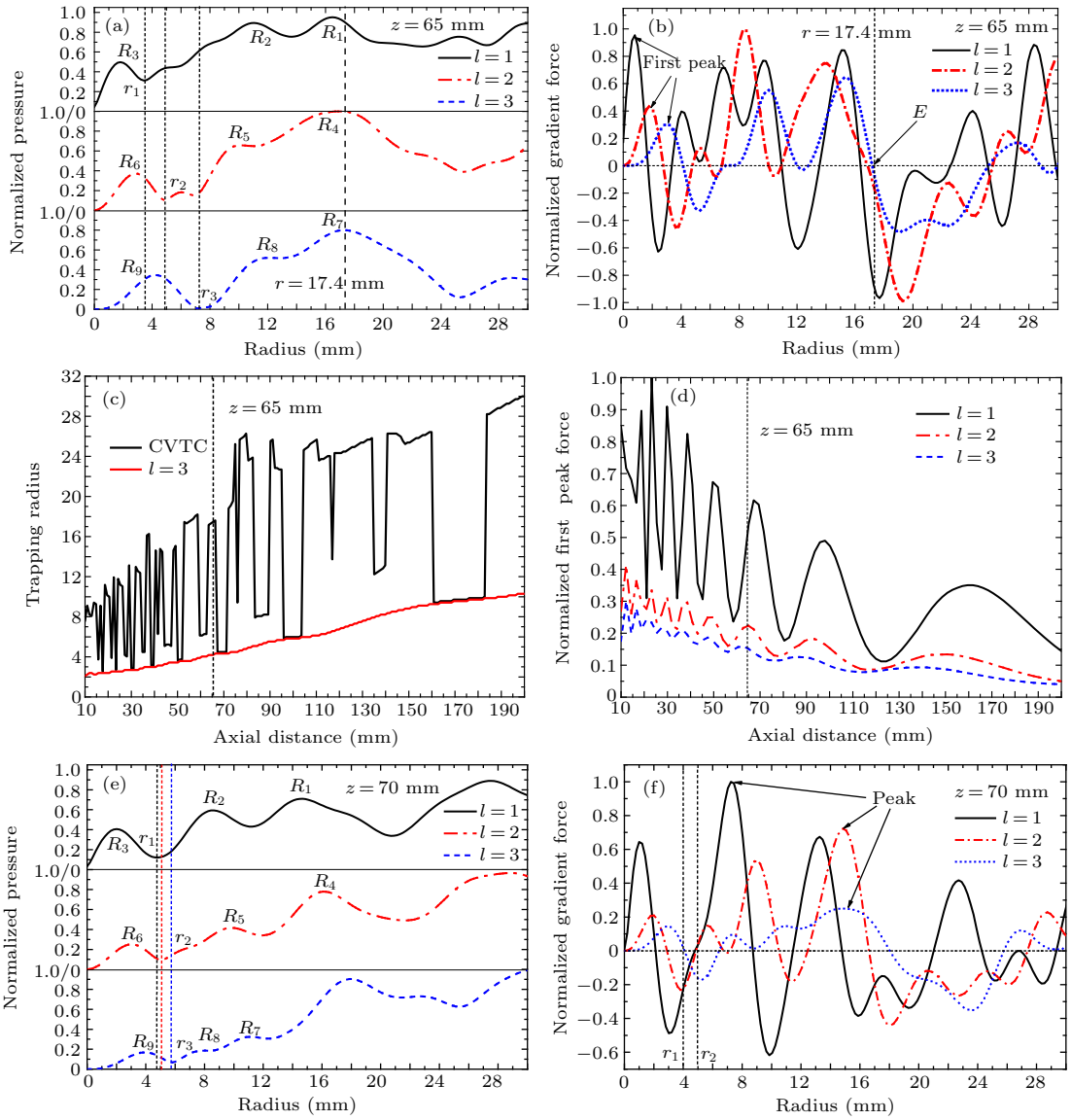


Fig. 3. Normalized radial distributions of (a) acoustic pressure and (b) AGF along the x-axis at $z = 65$ mm. Axial distributions of (c) the maximum trapping radius for AVs with the CVTC and $l = 3$ and (d) the first peak of radial AGF. Normalized radial distributions of (e) acoustic pressure and (f) AGF along the x-axis at $z = 70$ mm.

The higher AGF can be generated by paraxial AVs, although the acoustic pressure of the paraxial region is low. The 1-D distributions of AGF for three topological charges are shown in Fig. 3(b) along the x-axis positive direction. The AGF in the paraxial region is higher than that in the off-paraxial region. It should be noted that the positive value of AGF indicates the direction of the force toward the AV center, and the negative value is opposite to the positive value. Therefore, when the acoustic field has invariable topological charge $l = 1$, the particles are trapped into the vortex center only in the range of 1.8 mm. With the increase of the topological charge, the first peak of AGF decreases sharply, accordingly with an enlarged radius. It can be seen that the higher AGF is generated by the AVs with smaller topological charge, but the trapping radius is minimal. Because the AVs with CVTC can be spliced into a coherent whole with the positive radial AGF in the range of 0–17.4 mm, the trapping radius will be extended to 17.4 mm at axial distance $z = 65$ mm. Furthermore, regarding the particle size, the average diameter of particles up to 0.2 mm, which is 1/30 of the wavelength ($f = 500$ kHz), is successively trapped by the AVs.

The trapping radius is enlarged by the AVs with CVTC, which depends on the axial distance of the cross-section for trapping particles. In this part, the maximum trapping radius ($r_{\max}$) is defined as the longest radial distance from the vortex center to the location of the free-moving particle which can be moved to the vortex center. In order to calculate conveniently and accurately the maximum trapping radius, a logical expression is set up by applying comparison and OR logical that described as $s(r_n) = (F_1(r_n) > 0) \vee (F_2(r_n) > 0) \vee (F_3(r_n) > 0)$, where "$\vee$" respects OR logical operator, r_n is the radial distance from the vortex center to location of any free-moving particle, $F_l(r_n)$ is the AGF at the radial distance r_n when the topological charge $l = 1$, 2 or 3. As we know, when $s(r_n) = 0$,

three AGFs are all less than zero at radial distance r_n, which means the particle will be driven away from the vortex center by AVs with CVTC. However, when $s(r_n) = 1$, at least one of the AGF is greater than zero and can drive particles toward the vortex center. So in order for the particles to move to the vortex center, in the radial range of 0–$r_{\max}$, it is to make sure that all the $s(r_n)$ are equal to 1. The results of logical operation are all 1 in the radial range of $(0, r_n)$, and $s(r_{n+1}) = 0$, the maximum trapping radius is identified as $r_{\max} = r_n$.

The axial distributions of the maximum trapping radii for AVs with CVTC and $l = 3$ are shown in Fig. 3(c). Obvious fluctuations of trapping radii for AVs with CVTC are clearly displayed. With the increase of the axial distance, the trapping radius of AVs with CVTC shows a trend of fluctuating increase, and the trapping radius of AVs with $l = 3$ increases. It can be seen that there are several overlaps of two curves, for example, at $z = 67$–72 mm. In the overlap region, even the AVs with CVTC cannot enlarge the trapping radius. In addition, the axial regions with the short distance between two curves are observed, for instance, $z = 59$–62 mm. It indicates that the desired trapping radius is not generated by the AVs with CVTC at those axial distances. However, there are multiple axial regions with enlarged trapping radius in Fig. 3(c), such as $z = 62$–67 mm. The trapping range is enlarged by the AVs with CVTC at this axial region, demonstrating a large enough range for trapping particles. The trapping radius of the AVs with CVTC is 4.14 times of $l = 3$.

In addition, a higher AGF is required for efficient particle trapping. The axial distributions of the AGF for $l = 1$, 2, and 3 are plotted in Fig. 3(d), for each l, the axial distribution of the AGF for paraxial AVs exhibits a decreasing tendency with intense rapid fluctuations. However, in the smaller axial distance, the cross-section with higher AGF is not easy to trap particles in the practical application. Therefore, the AV at axial distance $z = 65$ mm which is characterized by relatively higher AGF for each l.

As mentioned above, not all of the cross-sections are suitable to trap particles for the AVs with CVTC, even in near-field where the AGF is higher, such as the axial distance $z = 70$ mm. When the topological charge is 2, assuming that the particles are trapped in the valley at the radial distance $r_2 = 5$ mm, as shown in Fig. 3(e). Since the acoustic pressures generated by AVs with three topological charges are all low in radial distance $r = 5$ mm, the particles cannot be trapped to the vortex center by AVs with CVTC. The 1-D distributions of AGF for three topological charges are shown in Fig. 3(f) at the axial distance $z = 70$ mm. The signs of AGF for three topological charges are all negative in the range of $r_1 = 4$ mm to $r_2 = 5$ mm, the particles in this range will be pushed away from the vortex center. In other words, successful trapping must satisfy that the AGFs produced by the three topological charges cannot be negative at the same time in a path of particle movement.

4. Experimental studies

As shown in Fig. 4(a), an 8-channel driving system was designed to excite the transducer arrays. An 8-element sector transducer array with a radius of 40 mm at the center frequency of 500 kHz was employed for the measurements. Controlled by the logical inputs from a field programmable gate array (FPGA) through a serial peripheral interface, the sinusoidal current outputs with programmable time delay (initial phase difference) were sent out synchronously from the high-speed ultrasound beamforming source drivers (MD2134, Supertex Inc., USA), and then amplified by high-voltage MOSFETs (DN2625, Supertex Inc., USA) to excite the respective sector transducers in turn. Also, controlled by the motion controller (Newport ESP301, Newport Corporation, USA), a needle hydrophone (Onda HNR-1000, diameter 1 mm, Onda Corporation, USA) mounted on a 3-D motion stage (Newport M-ILS250, Newport Corporation, USA) was used to measure the acoustic pressure. The detected waveform at each position was collected by a digital oscilloscope (Agilent DSO9064A, Agilent Corporation, USA) and saved in a computer for further signal processing.

In the experiments of trapping particles, polyethylene particles with a diameter of 0.2 mm are placed at the interface between a lower layer of water and an upper layer of edible oil. The particles are therefore sustained by buoyancy and gravity, and are either free to move in cross-section or fixed at axial distance $z = 65$ mm. The sector transducer array is located in the lowest layer at $z = 0$ mm. The trajectories of particles are recorded by the camera. The reflection and refraction of sound waves are ignored in transmission. The properties of the media and particle, i.e., density and speed of sound, are listed in Table 2. The dynamic acoustic field emitted by the sector transducer array repeatedly is used to trap particles in this experiment.

Table 2. List of material properties.

	Water	Oil	Particle
Density (kg/m^3)	1000	940	918
Velocity (m/s)	1500	1458	1900
Viscosity (Pa·s)	1.01×10^{-3}	0.95	

In order to enlarge the trapping range and improve the trapping efficiency, a new kind of drive signals of transducers is designed, which mades the topological charges of the AVs change periodically, $l = 3, 2, 1, 3, 2, 1 \ldots$. The duty cycles of the drive signals are different and adjustable for three topological charges. In the setup, the particles undergo an acoustic gradient force F and friction force $f_s = 6\pi\eta ru$, where u is the velocity of the particle and η is the viscosity of the medium surrounding the particle. According to Newton's second law,

the differential equation of the velocity of the particle is established in the layer between two liquids, $F - f_s = m\mathrm{d}u/\mathrm{d}t$. The particle initially at rest is submitted to a step of gradient at the time $t = 0$, its velocity as a function of time is expressed as $u(t) = \frac{F}{6\pi\eta r}\left[1 - \exp\left(-\frac{6\pi\eta r}{m}t\right)\right]$. The radial displacement can be calculated using

$$s = -\frac{F}{6\pi\eta r}t + \frac{Fm}{(6\pi\eta r)^2}\exp\left(-\frac{6\pi\eta r}{m}t\right) - \frac{Fm}{(6\pi\eta r)^2}.$$

It takes up to 40 s for the particles to be moved to any one of the valley. When $nT = 40$ s, the period of the drive signal is $T = 2 \times 10^{-6}$ s, so the number of the period for each topological charge is set as $n = 20 \times 10^6$ in the acoustic field with CVTC. The large-region trapping particles can be realized by the AVs with CVTC.

When the topological charge $l = 3$, the particles are trapped in the regions of annular valleys where the radial distances are $R_{31} = 7$ mm and $R_{32} = 22.7$ mm, particles could not be gathered in the vortex center, as shown in Fig. 4(b). The breadth of the valley between main lobes and side lobes is very narrow, a much smaller number of trapped particles are distributed on the radial distance $R_{32} = 22.7$ mm. A star-shaped pattern is formed by most of the particles. The particle ring of radius $R_{31} = 7$ mm is exactly located in the valley region between $R_8 = 12$ mm and $R_9 = 4.2$ mm (as shown in Fig. 2(a3)). When the topological charge $l = 2$, the particles are trapped in the regions of annular valleys where the radial distances are $R_{21} = 5$ mm and $R_{22} = 21.3$ mm, as shown in Fig. 4(c). The particles are distributed in the valley ($R_{22} = 21.3$ mm) between the main lobes and the side lobes, and a particle ring of radius $R_{21} = 5$ mm appears in the valley region between $R_5 = 10$ mm and $R_6 = 2.8$ mm (as shown in Fig. 2(a2)). When the topological charge $l = 1$, two particle rings are obviously displayed in Fig. 4(d) with the radii of $R_{11} = 3.8$ mm and $R_{12} = 18.1$ mm. The particle ring of radius $R_{11} = 3.8$ mm is exactly located in the valley region between $R_2 = 11$ mm and $R_3 = 1.8$ mm (as shown in Fig. 2(a1)). When the AVs with CVTC are excited by the same transducers, the dispersed particles are moved from the radial distance 17.4 mm to the vortex center, and finally gather in the vortex center, as shown in Fig. 4(e). Due to the orbital angular momentum carried by AVs, the particles in the vicinity of the vortex center rotate around the axis of the AVs.

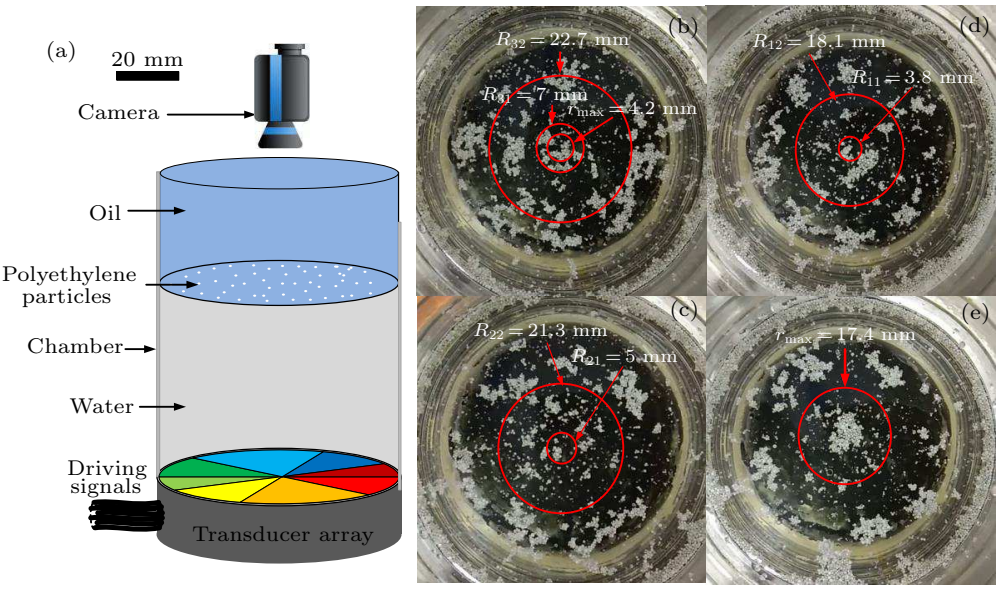


Fig. 4. Diagram of (a) experimental setup for trapping and rotating polyethylene particles using a 500 kHz sector transducer array at the base of a chamber filled with degassed water and oil. The distributions of polyethylene particles in the action of AV fields with topological charges (b) $l = 3$, (c) $l = 2$, (d) $l = 1$ and (e) continuously variable topological charges, at $z = 65$ mm. Multimedia view of (e): The experiment of trapping particles for (e).

5. Discussion

There are several points that deserve consideration in the experiments of trapping polyethylene particles. Firstly, polyethylene particles are unevenly distributed in the interface between oil and water before switching on the transducers. Secondly, the distribution of pressure will be affected by the layered media. Thirdly, the force between the particles comes from the static electricity which is carried by the particles themselves. Therefore, the distributions of particles are presented as irregular annulus, which are also influenced by the diameter and the number of the particles. In addition, the experimental error is also caused by the inconsistency of the sector transducers. Despite all that, the experimental results are almost consistent with simulation results.

The particles could be captured stably by the AV at a reduced translational speed because of the increased viscosity of the water and oil. Therefore, to achieve a higher efficiency, a new focusing field with a specific structure should be designed

based on either a focusing transducer or an acoustic lens,[45] which might improve the performance of AVs with CVTC in a larger region particle manipulation. In actual object manipulation using AVs, the different size particles trapping at the vortex center was accomplished by the radial AGF (trapping force) in the transverse plane,[46] and trapping both relatively dense and stiff particles and relatively light and soft particles was realized at the pressure maximum of the axisymmetric Bessel beam in the Rayleigh regime.[47,48] In truth, the effects caused by the beam parameters, object shape, and orientation on the trapping behaviors were revealed. Born approximation method was extended to analyze trapping forces exerted by two- and three-dimensional acoustic Bessel and vortex fields on spherical and non-spherical objects of arbitrary size.[49] The acoustic tweezers consisted of a circular 64-element ultrasonic array operating at 2.35 MHz which generated ultrasonic pressure fields in a millimeter-scale fluid-filled chamber.[38] The region where the particles were manipulated could only be in a certain plane inside the chamber, and particles outside the peak pressure could not be captured. The result of sweeping the particles into a single trap was achieved by reducing the topological charge but not the continuously variable topological charges.

Also as described above, an AV with CVTC can in theory capture particles in a larger region. The trapping radius of the AV should be selected based on the axial distance of the cross-section for trapping particles. For the present experimental system, the trapping radius of the AV with CVTC is around 17.4 mm at axial distance $z = 65$ mm, thereby showing great potential for targeted drug delivery.

6. Conclusion

This paper proposes a method of generating a dynamically varying AV with a CVTC in combination with theoretical calculations, numerical simulations, and experimental verifications. The pressure distributions of the AV with a fixed topological charge show that the particles will be bounded by the annular peak pressure formed by the side lobes of the sector transducers, and cannot move to the vortex center. Fortunately, the AV with a CVTC generated by a sector transducer array can realize the precise trapping of polyethylene particles in a large range. By changing the topological charge of the AV, particles positioned in the pressure valley can move towards the vortex center. The characteristics of AGF for AVs with different TCs are analyzed in the range of trapping radius, where the AGFs acting on the particle are always directed towards the vortex center. The axial distribution of trapping radii is discussed, and the axial distance of $z = 65$ mm is identified as the optimal capture position. The system of a 8-element sector transducer array and a 8-channel driving circuit is designed to trap particles in a larger region.

This method is executable proved by the distributions of polyethylene particles trapped by AVs with four TCs. The bothersome issue of particles bounded in the region of annular pressure valleys can be solved by the AV with a CVTC, it allows particles trapped by side lobes to move to the vortex center. This study dexterously and independently manipulate multiple particles of millimeter level, which suggests potential applications of particles trapping in biomedical engineering, such as the adjuvant treatment of calculi disease and targeting drug delivery.

Acknowledgment

Project supported by the National Key R&D Program of China (Grant No. 2023YFE0201900).

References

[1] Haake A and Dual J 2002 *Ultrasonics* **40** 317
[2] Foresti D, Sambatakakis G, Bottan S and Poulikakos D 2013 *Sci. Rep.* **3** 3176
[3] Marzo A, Seah S, Drinkwater B, Sahoo D, Long B and Subramanian S. 2015 *Nat. Commun.* **6** 8661
[4] Drinkwater W, Seah A, Malkin R, Subramanian S and Carter T 2014 *IEEE Trans. Ultrason. Ferroelectr. Freq. Control* **61** 1233
[5] Xie W and Wei B 2001 *Appl. Phys. Lett.* **79** 881
[6] Hong Z, Xie W and Wei B 2011 *Rev. Sci. Instrum.* **82** 074904
[7] Xie W, Cao C, Lü Y, Hong Z and Wei B 2006 *Appl. Phys. Lett.* **89** 214102
[8] Kozuka T, Yasui K, Tuziuti T, Towata A and Iida Y 2006 *J. Acoust. Soc. Am.* **120** 3370
[9] Marston P 2009 *J. Acoust. Soc. Am.* **125** 3539
[10] Cain C and Umemura S 1986 *IEEE Trans. Microwave Theory Tech.* **34** 542
[11] Bernassau A, Courtney C, Beeley J, Drinkwater B and Cumming D 2013 *Appl. Phys. Lett.* **102** 16410
[12] Nye J and Berry M 1974 *Proc. R. Soc. London* **336** 165
[13] Thomas J and Marchiano R 2003 *Phys. Rev. Lett.* **91** 244302
[14] Hong Z, Zhang J and Drinkwater B 2015 *Phys. Rev. Lett.* **114** 214301
[15] Volke-Sepúlveda K, Santillán A and Boullosa R 2008 *Phys. Rev. Lett.* **100** 024302
[16] Dashti P, Alhassen F and Lee H 2006 *Phys. Rev. Lett.* **96** 043604
[17] Zhang L and Marston P 2011 *Phys. Rev. E* **84** 035601(R)
[18] Anhaüser A, Wunenburger R and Brasselet E 2012 *Phys. Rev. Lett.* **109** 034301
[19] Leão-Neto J and Silva G 2016 *Ultrasonics* **71** 1
[20] Mitri F, Lobo T and Silva G 2012 *Phys. Rev. E* **85** 026602
[21] Meng L, Cui X, Dong C, Liu X, Wei Zhou, Zhang W, Wang X, Niu L, Li F, Cai F, Wu J and Zheng H 2020 *Appl. Phys. Lett.* **116** 073701
[22] Mitri F 2014 *IEEE Trans. Ultrason. Ferroelectr. Freq. Control* **61** 2089
[23] Zheng H, Gao, Ma Q, Dai Y and Zhang D 2014 *J. Appl. Phys.* **115** 084909
[24] Yang L, Ma Q, Tu J and Zhang D 2013 *J. Appl. Phys.* **113** 154904
[25] Gao L, Zheng H, Ma Q, Tu J and Zhang D 2014 *J. Appl. Phys.* **116** 024905
[26] Baresch D, Thomas J and Marchiano R 2013 *J. Appl. Phys.* **113** 184901
[27] Marchiano R and Thomas J 2005 *Phys. Rev. E* **71** 066616
[28] Li Y, Guo G, Ma Q, Tu J and Zhang D 2017 *J. Appl. Phys.* **121** 164901
[29] Du L, Hu G, Hu Y and Wang Q 2023 *Sensors* **23** 6874
[30] Wang Q, Li Y, Ma Q, Guo G, Tu J and Zhang D 2018 *J. Appl. Phys.* **123** 034901
[31] Pazos-Ospina J, Quiceno F, Ealo J, Muelas H and Camacho J 2015 *Phys Procedia* **70** 183
[32] Jiménez N, Sánchez-Morcillo, PicóR, Garcia-Raffi L, Romero-Garcia V and Staliunas K 2015 *Phys. Procedia* **70** 245

[33] Jiang X, Zhao Ji, Liu S, Liang B, Zou X, Yang J, Qiu C and Cheng J 2016 *Appl. Phys. Lett.* **108** 203501
[34] Jiang X, Li Y, Liang B, Cheng J and Zhang L 2016 *Phys. Rev. Lett.* **117** 034301
[35] Cai F, He Z, Liu Z, Meng L, Cheng X and Zheng H 2011 *Appl. Phys. Lett.* **99** 253505
[36] Wang T, Ke M, Li W, Yang Q, Qiu C and Liu Z 2016 *Appl. Phys. Lett.* **109** 123506
[37] Courtney C, Drinkwater B, Demore C, Cochran S, Grinenko A and Wilcox P 2013 *Appl. Phys. Lett.* **102** 123508
[38] Courtney C, Demore C, Wu H, Grinenko A, Wilcox P, Cochran S and Drinkwater B 2014 *Appl. Phys. Lett.* **104** 154103
[39] Hong Z, Zhang J and Drinkwater B 2015 *Europhys. Lett.* **110** 14002
[40] Glynne-Jones P, Démoré C, Ye C, Qiu Y, Cochran S and Hill M 2012 *IEEE Trans. Ultrason. Ferroelectr. Freq. Control* **59** 1258
[41] Baresch D, Thomas J and Marchiano R 2016 *Phys. Rev. Lett.* **116** 024301
[42] Baresch D, Thomas J and Marchiano R 2013 *J. Appl. Phys.* **113** 184901
[43] Bruus H 2012 *Lab Chip* **12** 1014
[44] Wooh S and Shi Y 1998 *Ultrasonics* **36** 737
[45] Wang Q, Hu Y, Wang S and Li H 2023 *Chin. Phys. B* **32** 064304
[46] Zhou C, Wang Q, Pu S, Li Y, Guo G, Chu H, Ma Q, Tu J and Zhang D 2020 *J. Appl. Phys.* **128** 084901
[47] Fan X and Zhang Li 2019 *Phys. Rev. Appl.* **11** 014055
[48] Fan X, Zhu Y, Su Z, Li N, Huang X, Kang Y, Li C, Weng C, Zhang H, Kan W and Assouar B 2023 *Phys. Rev. Appl.* **19** 034032
[49] Fan X and Zhang L 2023 *J. Acoust. Soc. Am.* **154** 3354